

PAPER • OPEN ACCESS

# Parametric study of Alfvénic instabilities driven by runaway electrons during the current quench in DIII-D


To cite this article: A. Lvovskiy *et al* 2023 *Nucl. Fusion* **63** 046011

View the [article online](#) for updates and enhancements.

You may also like

- [Generation and dissipation of runaway electrons in ASDEX Upgrade experiments](#)  
G. Pautasso, M. Dibon, M. Dunne et al.
- [Runaway electron beam control](#)  
D Carnevale, M Ariola, G Artaserse et al.
- [Full conversion from ohmic to runaway electron driven current via massive gas injection in the TCV tokamak](#)  
J. Decker, G. Papp, S. Coda et al.

# Parametric study of Alfvénic instabilities driven by runaway electrons during the current quench in DIII-D

A. Lvovskiy<sup>1,\*</sup> , C. Paz-Soldan<sup>2</sup> , N.W. Eidietis<sup>1</sup> , A. Dal Molin<sup>3</sup> ,  
G.H. DeGrandchamp<sup>4</sup> , E.M. Hollmann<sup>5</sup> , J.B. Lestz<sup>1,4</sup> , C. Liu<sup>6</sup> , M. Nocente<sup>7</sup> ,  
D. Shiraki<sup>8</sup> and X.D. Du<sup>1</sup> 

<sup>1</sup> General Atomics, San Diego, CA, United States of America

<sup>2</sup> Columbia University, New York, NY, United States of America

<sup>3</sup> Institute for Plasma Science and Technology, NRC, Milan, Italy

<sup>4</sup> University of California, Irvine, Irvine, CA, United States of America

<sup>5</sup> University of California San Diego, La Jolla, CA, United States of America

<sup>6</sup> Princeton Plasma Physics Laboratory, Princeton, NJ, United States of America

<sup>7</sup> University of Milan-Bicocca, Milan, Italy

<sup>8</sup> Oak Ridge National Laboratory, Oak Ridge, TN, United States of America

E-mail: [lvovskiya@fusion.gat.com](mailto:lvovskiya@fusion.gat.com)

Received 26 August 2022, revised 10 January 2023

Accepted for publication 30 January 2023

Published 1 March 2023



## Abstract

To avoid or mitigate runaway electron (RE) beams in ITER, RE-driven instabilities are actively studied as a complimentary technique to massive material injection. In this work we report experimental dependencies of Alfvénic instabilities driven by REs during the current quench in DIII-D on plasma and material injection parameters. These instabilities, observed in the frequency range of 0.1–3 MHz, correlate with increased RE loss and thus may play a role in non-sustained RE beams. It was found that as the toroidal magnetic field ( $B_T$ ) decreases, the RE population becomes more energetic, the energy of instabilities increases, and no RE beam is observed when the maximum energy of REs exceeds 15 MeV (or when  $B_T$  is below 1.8 T). Analysis of disruptions at plasma core temperature ( $T_e$ ) of 1 keV and 8 keV shows that the RE population is much less energetic (with the maximum energy of only about 3 MeV) when  $T_e$  is high, and no instabilities are observed in this case. Besides disruptions above caused by Ar injection, cases with Ne and D<sub>2</sub> injections were also studied. Both Ne and D<sub>2</sub> injections cause no sustained RE beams, however, for different reasons. Measurements of the instability polarization indicate that it is of predominantly compressional nature at the edge, which is consistent with modeling suggesting excitation of compressional Alfvén eigenmodes. However, drive of global Alfvén eigenmodes is also possible at low frequencies.

Keywords: runaway electrons, kinetic instabilities, tokamak disruptions

(Some figures may appear in colour only in the online journal)

\* Author to whom any correspondence should be addressed.



Original Content from this work may be used under the terms of the [Creative Commons Attribution 4.0 licence](https://creativecommons.org/licenses/by/4.0/). Any further distribution of this work must maintain attribution to the author(s) and the title of the work, journal citation and DOI.

## 1. Introduction

Avoidance or dissipation of runaway electron (RE) beams in ITER and future high current tokamaks is of urgent and critical importance [1, 2]. Despite the fact that shattered pellet injection has been adopted as the baseline disruption mitigation scheme for ITER [3], alternative or complimentary techniques focused on RE dissipation are also being actively studied. Among them are RE beam safe loss via MHD instability [4–6], RE deconfinement via disruption-excited passive 3D coil [7, 8], and RE dissipation via launching of external waves [9]. The latter search is motivated by the discovery of kinetic instabilities driven by REs during the current quench (CQ) in DIII-D [10] and similar instabilities in ASDEX Upgrade [11]. It was also predicted that alpha particles can drive kinetic instabilities during the CQ in ITER scattering REs off the plasma [12]. Mitigation techniques expelling REs from plasma during the CQ are very appealing since unlike an impurity injection they can help to reduce high avalanche gain in high current tokamaks.

On DIII-D, it was observed that kinetic instabilities correlate with increased RE loss, and when their energy exceeds some threshold no sustainable RE beam can be generated. It was also measured that the power of instabilities increases as the RE population becomes more energetic, and such actuators as increasing pre-disruption plasma current and decreasing amount of injected argon (used to deliberately trigger the disruption) both increase the energy of REs. The frequency of instabilities (magnetic fluctuations) was found to be within 0.1–3 MHz, which corresponds to  $f/f_{ci} \approx 0.1\text{--}3.6$ , where  $f_{ci}$  is ion cyclotron frequency. Based on the frequency analysis, compressional Alfvén eigenmodes (CAEs) were proposed as the candidate instability, which was later supported by modeling [13]. According to this modeling, CAEs can be driven by barely passing and trapped REs, formed via collisions with plasma impurities enhancing the pitch angle scattering. Resonant REs excite CAEs through the gradient of the distribution function in the momentum space and radial direction. Interaction with CAEs increases the radial transport of REs. As shown in more recent simulations [14], strong instabilities can produce large-amplitude perpendicular magnetic fluctuations ( $\delta B_{\perp}$ ), and the overlap of multiple modes can lead to diffusion of both resonant and non-resonant REs on the timescale of a few milliseconds.

In this paper we report observation of Alfvénic instabilities driven by REs during the CQ in DIII-D depending on the plasma, material injection and RE parameters. In section 3 we document the dependence on the toroidal magnetic field, in section 4 we present the effect of the pre-disruption plasma electron temperature, in section 5 we report massive gas injections (MGIs) of species other than argon (such as neon and deuterium, but do not study mixture of gases to ease execution and interpretation of experiments), and in section 6 we present measurements of the polarization and toroidal mode number of instabilities.

## 2. Experimental setup

These experiments have been performed on the DIII-D tokamak [15] using an inner wall limited, electron cyclotron heated ohmic plasma deliberately disrupted via massive material injection. Plasma current, toroidal magnetic field, electron temperature and parameters of a material injection specific to every experiment are listed in the separate sections below. Since plasma diagnosis during disruptions, when its parameters change by many orders of magnitude on a millisecond time scale, is very challenging, we relied only on a limited set of diagnostics. The magnetic fluctuations caused by Alfvénic instabilities were measured using a recently upgraded radio frequency (RF) magnetic diagnostic [16], with three toroidal magnetic loops (separated by  $13.1^{\circ}$  and  $17.6^{\circ}$ ) located at the outer mid-plane providing a toroidal mode number and two orthogonal loops located at the outer wall providing polarization. The RF diagnostic is not absolutely calibrated, has a cut-off below 0.1 MHz, and can measure without aliasing up to 100 MHz. The hard x-ray (HXR) bremsstrahlung radiation from confined REs was measured using a collimated tangential single central sight-line of the gamma ray imager (GRI) [17–22] equipped with a LYSO:Ce gamma-ray detector [23] (the noise floor was taken at 0.5 MeV). The volumetric HXR signal was measured by a distant scintillating detector (BC-400) sensitive to HXRs with energy above 5 MeV [24]; when this signal becomes spiky, we interpret this change as RE loss to the wall. Edge plasma cooling was measured using an edge channel of the electron cyclotron emission (ECE) radiometer (87.5 GHz, second harmonic, X-mode) [25]. Core plasma cooling free of the density cut-off was measured using the third harmonic broadband ECE diagnostic [26]. The line-integrated electron density  $\langle n_e l \rangle$  was measured using a mid-plane radial chord of the CO<sub>2</sub>-interferometer [27].

## 3. Dependence of Alfvénic instabilities and RE generation on $B_T$

### 3.1. Motivation

There is a well-known threshold on toroidal magnetic field  $B_T > 2\text{--}2.2$  T for RE beam generation [28]. This is not a hard limit (for example KSTAR and J-TEXT reported occasional generation of RE beams at  $B_T$  being as low as 1.3 T [29] and 1.2 T [30], respectively), but rather an operational guidance to reliably achieve a sustainable RE beam. Though later it was suggested that the ratio of magnetic fluctuations to toroidal magnetic field  $\delta B/B_T > 10^{-4}\text{--}10^{-3}$  is likely a more relevant metric for a non-sustained RE beam than a low  $B_T$  itself [31, 32].

Since the dispersion relation of Alfvénic instabilities scales with the toroidal magnetic field as  $\omega \propto B_T$ , it is possible that the  $B_T$  threshold can relate to these instabilities. For example, decreasing  $B_T$  may lead to their frequency shifting to lower values which can change the resonant condition between instabilities and REs and affect the RE loss.

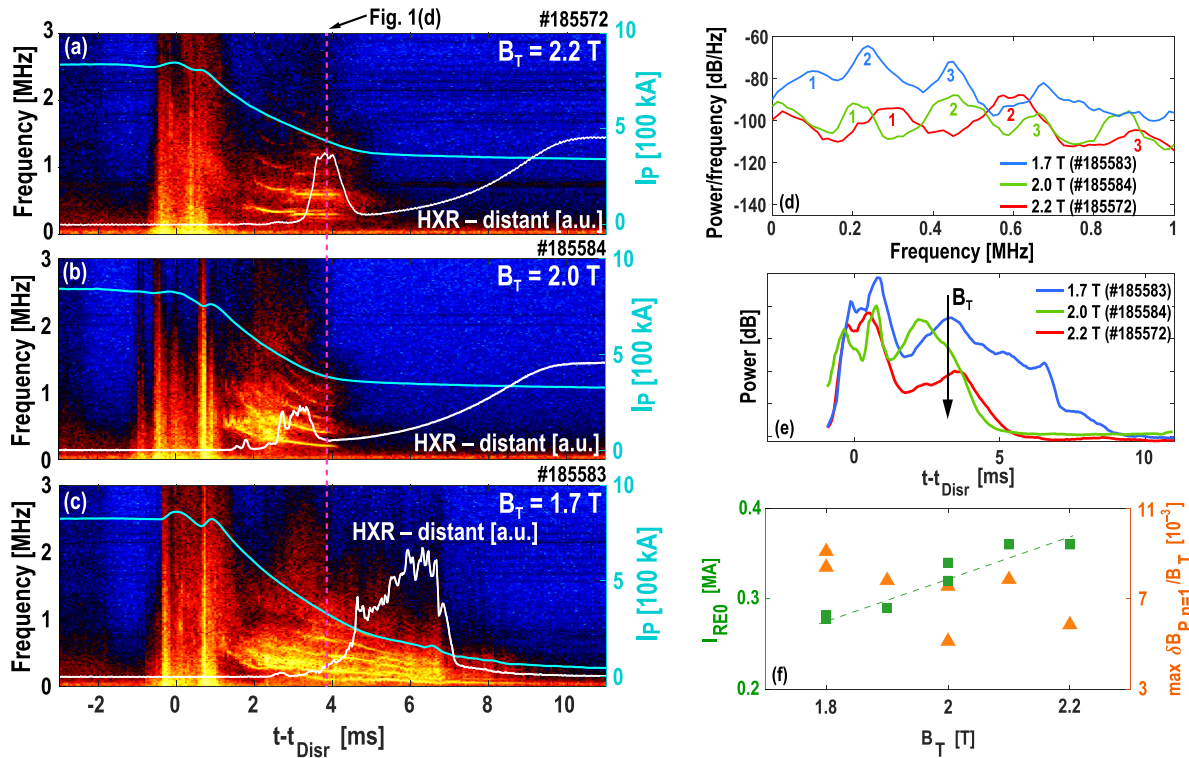


**Figure 1.** (a)–(c) Spectrograms of magnetic fluctuations during the CQ for plasma with different  $B_T$ , (d) power spectral density of magnetic fluctuations along the vertical dash line (time average window is  $50 \mu\text{s}$ ) shown in panels (a)–(c), (e) power of magnetic fluctuations calculated in the range of 0.1–3 MHz, (f) dependence of the RE current, measured in 10 ms after  $t_{\text{Disr}}$ , on  $B_T$  (the dash line is to guide the eye only) and the maximum amplitude of  $n = 1$  mode of poloidal magnetic fluctuations measured at the LFS midplane and normalized to  $B_T$  at the wall. Disruptions were caused by 160 Torr·L of Ar MGI. The smooth increase of the HXR bremsstrahlung signal after the CQ can be explained by the continuing influx of argon and, though to lesser extent than during the CQ, by increasing RE current replacing the thermal current. The avalanche gain during the CQ is expected to be about a factor of 5 [34]; the RE current reaches a plateau when the collisional damping balances acceleration by the electric field.

Moreover, Alfvénic instabilities typically become stronger with increasing Alfvénic Mach number ( $v/v_A$ , where  $v$  is a characteristic velocity of REs driving the instability and  $v_A$  is Alfvénic velocity), which is inversely proportional to  $B_T$ . For example, increasing growth rate of RE-driven toroidal Alfvén eigenmodes (TAEs) as  $B_T$  decreases was found in [33]. In this section we report how  $B_T$  affects the Alfvénic instabilities and RE generation.

### 3.2. Experiment

To study the  $B_T$  effect, a typical scenario of the RE experiment on DIII-D was employed: plasma current  $I_p = 0.8 \text{ MA}$ , plasma core temperature  $T_e = 1\text{--}2 \text{ keV}$ , Ar MGI in the amount of 160 Torr·L. The only varied parameter was  $B_T$  changing from 2.2 T to 1.6 T (this corresponds to a pre-disruption edge safety factor changing from 5 to 3.9). No sustainable RE beam was observed for  $B_T < 1.8 \text{ T}$ .

Spectrograms of toroidal magnetic field fluctuations measured during the CQ for three cases when  $B_T$  equals 2.2 T, 2.0 T, and 1.7 T are shown in figures 1(a)–(c), respectively. It can be seen that the separate modes of instabilities shift as a whole to lower frequencies and the spacing between them decreases

while the RE loss becomes more intermittent. The maximum measured frequency of modes decreases from about 2 MHz to 1 MHz. The longest and brightest modes are observed for the case with lowest  $B_T$  and without sustainable RE beam. The time of disruption  $t_{\text{Disr}}$  here and later is defined as the moment of an  $I_p$  spike.

Single vertical slices of these spectrograms taken in 4 ms after the disruption, when the frequency of the modes changes slower than in the beginning of the CQ, are shown in figure 1(d). The lowest frequency mode (denoted by ‘1’) is located at 0.1 MHz, 0.21 MHz, 0.29 MHz and the spacing between modes equals to 0.19 MHz, 0.22 MHz, 0.31 MHz for  $B_T$  equal 1.7 T, 2.0 T, and 2.2 T, respectively. The power of modes over time, calculated in the range of 0.1–3 MHz, is shown in figure 1(e). It can be seen there that decreasing magnetic field not only reduces the frequency and spacing of modes, but also increases their power. The post-CQ RE current  $I_{\text{RE0}}$ , measured in 10 ms after the disruptions, is shown in figure 1(f). Its magnitude increases from 0.28 MA to 0.36 MA as  $B_T$  increases from 1.8 T to 2.2 T. We consider  $I_{\text{RE0}}$  as predominantly runaway current since cold post-disruption bulk plasma ( $T_e \approx 1 \text{ eV}$ , measured by Thomson scattering in 15 ms after the disruption) implies much higher resistance (about

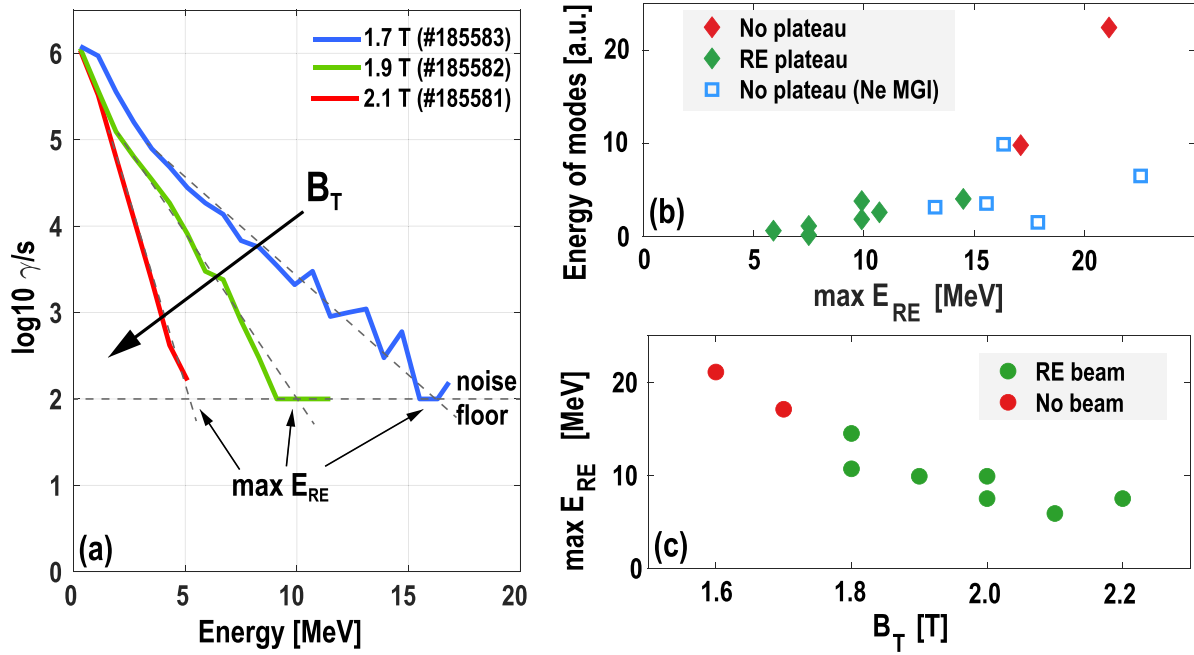


**Figure 2.** (a) HXR bremsstrahlung spectra from REs obtained over the CQ (integration window is 10 ms after disruptions) at different  $B_T$ , (b) dependence of the energy of kinetic instabilities on the maximum energy of REs, (c) dependence of the maximum energy of REs on  $B_T$ . The disruptions were caused by 160 Torr-L of Ar MGI except for the Ne MGI cases (section 5) overplotted in panel (b). The same integration time window is used for all HXR spectra to ease their comparison since reducing counting statistics for discharges with sustained RE beam does not qualitatively change the observed dependence (the same spectra, but with poorer counting statistics, are obtained with a 5 ms integration window).

1 m $\Omega$ , assuming Spitzer resistivity) than the resistance calculated from the measured current (about 300 kA) and loop voltage (about 10 V) and equal to 30  $\mu\Omega$ . The plasma power balance in this case is dominantly set between collisional heating and argon line radiation [35, 36].

The observed change of the power of kinetic instabilities could be solely associated with the magnetic field as it modifies the dispersion relation, growth rate, and resonance condition. However, as it was shown in [10], their power can also depend on the energy of REs. To compare the energy of REs, the energy spectra of the HXR bremsstrahlung radiation from REs obtained during 10 ms after the disruptions are shown in figure 2(a). There is clear difference between them for discharges taken at different  $B_T$ : as  $B_T$  increases, the HXR spectra soften and the maximum energy of HXRs decreases from 15 MeV to 5 MeV. Since deconvolution of HXR energy spectra to RE energy spectra is complicated during the CQ with continuously changing magnetic equilibrium, we take the maximum HXR energy as a convenient 0D metrics to compare how energetic the total RE population during the CQ. Simple idea that the HXR energy does not exceed the energy of REs allows us to use max  $E_{HXR}$  as max  $E_{RE}$ . The energy of the modes, calculated over the duration of instabilities, is plotted as a function of max  $E_{RE}$  in figure 2(b). It non-linearly increases as max  $E_{RE}$  increases. No RE beam is observed when max  $E_{RE}$  exceeds 15 MeV. Notably, max  $E_{RE}$  inversely correlates with  $B_T$ : as shown in figure 2(c), decreasing  $B_T$  leads to a more energetic RE population.

### 3.3. Discussion and conclusions

The results of the RE beam generation at different  $B_T$  clearly show that Alfvénic instabilities play a role here and they can at least partially explain the empirical observations that probability of a sustained RE beam increases with increasing  $B_T$ . It is found that the frequency of separate modes decreases (which changes the resonance condition), their spacing decreases (which may ease mode overlap), and the power of modes increases as  $B_T$  decreases. All of these changes can affect the instability drive as well as the scattering of REs from the plasma. Since it is complicated to isolate and weigh their individual effects on the RE loss experimentally, this will need to be addressed in future simulations. Notably, the simultaneous decrease in  $B_T$  and increase in max  $E_{RE}$  would both act to increase  $v/v_A$ , which Alfvénic instabilities typically favor.

It is also important to note that the dependence of RE energy on  $B_T$  is not understood. Presumably, the magnetic field magnitude affects the conversion of plasma current to RE current (during both seed and avalanche phases), and as it decreases, smaller population of REs needs to be accelerated to higher energy in attempt to replace the decaying plasma current (besides the observed decreasing  $I_{RE0}$  as  $B_T$  decreases, this is also supported by the maximum loop voltage linearly decreasing from 39 V to 29 V as  $B_T$  increases from 1.8 T to 2.2 T). As a result, the more energetic RE population may drive more powerful instabilities and effectively ‘kill’ itself in a vicious cycle via increased radial transport

due to scattering on magnetic perturbations produced by these instabilities. These observations are consistent with results reported on JET, where decreasing  $B_T$  correlated with decreasing runaway current and increasing accelerating electric field [37]. Also increasing magnetic fluctuations as  $B_T$  decreases were measured there during the CQ.

The reduced current conversion could hypothetically happen due to Alfvénic instabilities themselves. However, as reported in literature, it may also happen due to increased growth rate of whistler instabilities [38–40] (leading to increased pitch-angle scattering mitigating RE generation [41–43]) as well as decreased on-axis current density (leading to lower post-thermal electric field and weaker primary RE generation) [40]. Though we should note that no whistler instabilities were observed in this experiment. And despite they could be overlooked due to excitation at very high frequency, no direct RE loss driven by whistlers was documented in the past dedicated experiments [44, 45] or shown theoretically to explain the observed intermittent RE loss to the wall during the CQ.

Finally, we would like to mention the effect of MHD instabilities on the current conversion. It is expected that the MHD activity during the TQ may affect seed RE generation. In these experiments, the peak amplitude of  $n = 1$  mode of poloidal magnetic fluctuations ( $\delta B_{p,n=1}$ ), measured at the low field side (LFS) midplane during the TQ, was about 100–120 G. Its value, normalized to  $B_T$  at the measurement location, is shown in figure 1(f) as a function of  $B_T$ . Since it is difficult to see any clear dependence of  $\delta B_{p,n=1}$  on  $B_T$  without collecting more statistics, presently we assume that decreasing  $B_T$  does not increase MHD instabilities during the TQ and thus it does not affect seed RE generation via increased RE loss.

## 4. Alfvénic instabilities at reactor-relevant temperature

### 4.1. Motivation

Previously, no effect of the pre-disruption electron temperature  $T_e$  on the RE generation and kinetic instabilities has been found [10]. However, that study was limited by maximum  $T_e = 4$  keV. To access the reactor-relevant temperature  $T_e \approx 10$  keV, a new scenario, based on formation of the internal transport barrier, has been developed [34] following theoretical works on so-called hot tail generation [46–48]. At such temperature, the conversion of thermal to runaway current increases from typical DIII-D value of 20%–40% to nearly 100%. In this respect, it is interesting to study how this changes the RE distribution and drive of kinetic instabilities.

### 4.2. Experiment

In this experiment the pre-disruption core  $T_e$  was varied from 1 keV to 8 keV, while all other parameters ( $I_p = 0.6$  MA,  $B_T = 2.2$  T, argon ‘killer’ pellet injection of 14 Torr·L to trigger the disruption) were kept constant.

Two extreme cases are shown in figures 3(a) and (b): a disruption at  $T_e = 1$  keV leading to the RE beam with conversion of 20% and a disruption at  $T_e = 8$  keV resulting into 80% conversion of thermal to RE current. It can be also seen that besides remarkably different post-disruption RE currents, these cases show almost opposite magnetic activities. The disruption at  $T_e = 1$  keV is accompanied by moderate magnetic activity with a weak single mode, while the disruption at  $T_e = 8$  keV does not show any noticeable rise of magnetic fluctuations: magnetic signatures before and after the disruption look very similar to each other. Relatively weak magnetic activity without many clear modes observed even in the ‘cold’ case is often documented after Ar killer pellet compared to Ar MGI, as discussed in [10].

The HXR spectra for ‘cold’ and ‘hot’ disruptions are shown in figure 3(c). Lower pre-disruption  $T_e$  leads to clearly harder HXR spectra with maximum HXR (RE) energy about 5 MeV, while higher pre-disruption  $T_e$  corresponds to much softer HXR spectra with twice less maximum HXR (RE) energy. We should note that even discharges with the hardest HXR spectra have the maximum energy barely reaching the lowest energy observed in the  $B_T$  experiment with Ar MGI, where low and mid-energetic RE populations correlated with sustained RE beams (section 3).

### 4.3. Discussion and conclusions

The experiment on RE generation in discharges with high and low pre-disruption  $T_e$  shows that the high  $T_e$  discharges have greater conversion of plasma to RE current than the low  $T_e$  discharges and also lead to less energetic RE population and no signs of kinetic instabilities during the CQ. These observations are consistent with the model [48] predicting increasing current conversion and decreasing electron acceleration as the temperature increases. This result also does not contradict the hypothesis proposed in section 3 to explain the dependence of RE energy on  $B_T$ . Namely, that decreasing magnetic field presumably decreases the conversion of thermal to RE current, which leads to increased RE energy and increased power of kinetic instabilities further increasing the RE loss. In this paper we do not calculate the wave damping and kinetic drive at high  $T_e$  to explain theoretically the lack of instabilities at reactor-relevant temperature. Such task is out of the scope of this work, and we leave it for future. However, we would like to note that modeling at low  $T_e$  [13] points out the necessity of higher energy REs to observe the excitation of instabilities. This is required to satisfy the resonant condition between REs and plasma waves, since the precession frequency of trapped REs, driving the instabilities, depends on their energy.

## 5. Ne MGI and D<sub>2</sub> MGI quantity scan

### 5.1. Motivation

Historically, injections of impurities other than Ar have not led to generation of a sustained deliberate post-disruption

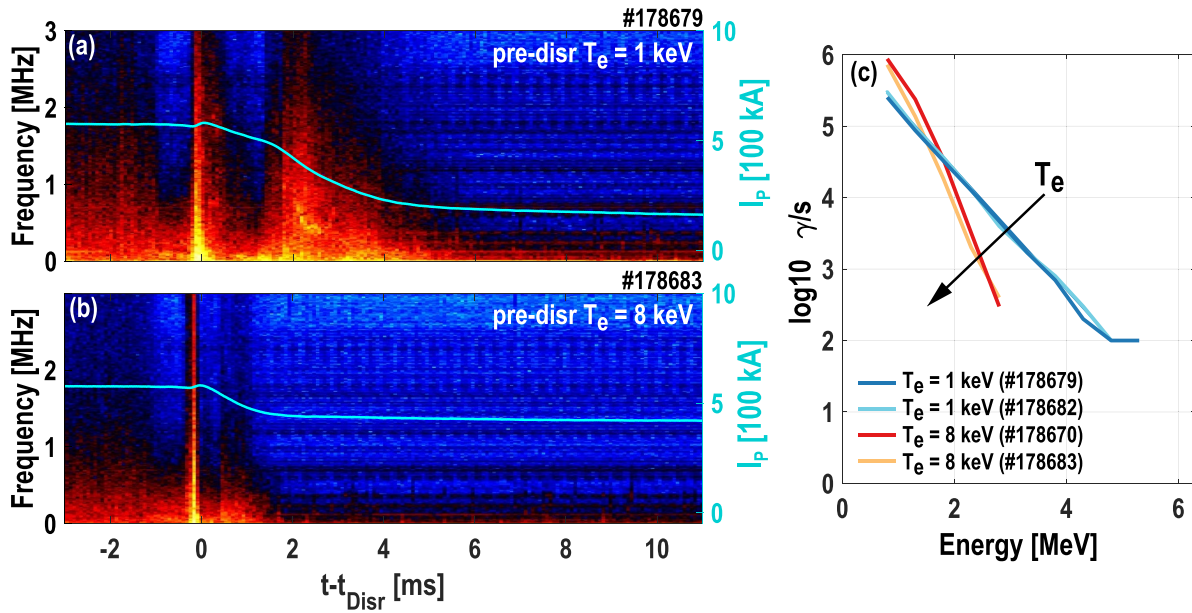


**Figure 3.** (a) and (b) spectrograms of toroidal magnetic field fluctuations in the discharge with pre-disruption core  $T_e = 1$  keV and  $T_e = 8$  keV, respectively, (c) HXR bremsstrahlung spectra from REs obtained over the CQ (integration window is 10 ms after disruptions) in discharges with different pre-disruption  $T_e$ .

RE beam in DIII-D (recently it was discovered that C influx from the wall into a high-temperature target plasma with  $T_e > 10$  keV can also produce a lower energy RE beam [34]). Consequently, such scenarios were abandoned in favor of the Ar pellet injection and Ar MGI. In order to investigate whether the instabilities driven by REs during the CQ and scattering REs off the plasma may play a role after injections of Ne or  $D_2$ , we revisited these cases owing the improved diagnostic coverage with the upgraded GRI and RF diagnostic.

## 5.2. Experiment

Parameters of the target plasma were the same as in the experiment with Ar MGI described in section 3. The only difference was the injected species,  $D_2$  MGI and Ne MGI. The amounts injected were varied from 100 Torr-L to 800 Torr-L.

**5.2.1. Disruptions caused by Ne MGI.** As in the past, no sustained RE beam was observed after Ne MGI. However, both RE population and Alfvénic instabilities were diagnosed during the CQ. The Alfvénic instabilities seen in magnetic spectrograms as separate modes in the range from 0.1–3 MHz were the most clear and longest-duration of all cases studied before. The energy of instabilities after Ne MGI is by factor of 10 greater than for similar Ar MGI cases (with the same  $B_T$  and amount injected).

Two disruptions, with injections of 110 Torr-L and 740 Torr-L of Ne are shown in figures 4(a) and (b), respectively. It can be seen, that the greater injection leads to instabilities shifted to lower frequencies. This is expected since the frequency of Alfvénic instabilities decreases as the ion density increases (or the electron density, assuming

plasma quasineutrality). The same dependence should explain gradually decreasing frequency of modes during the CQ after impurity injection. Though verification of the scaling  $f \propto n_i^{-1/2}$  is not possible during the CQ due to unknown density distribution as well as the lack of assurance that the other plasma parameters stay the same. As the amount injected increases, the RE population becomes less energetic as shown in figure 4(c). This effect is similar to cases with increasing amount of Ar MGI [10] and may be explained by increased collisional damping of REs. However, compared to Ar MGI, Ne MGI does not reduce the energy of the RE population to the same extent; even at the maximum injected amount of Ne, the maximum energy of REs is still about 13 MeV (which for a similar Ar MGI case would typically cause no sustained RE beam). This weak and not understood effect of the injected Ne amount on the energy of REs or poor statistics may be a reason of the vague dependence of maximum RE energy on the energy of instabilities observed in the experiment and shown in figure 2(b).

Despite relatively energetic RE population after Ne MGI may lead to somewhat elevated energy of instabilities during the CQ, which could increase the RE loss and prevent formation of a sustained RE beam, the role of these instabilities is assumed to be minor here. This can be seen from the comparison of disruptions caused by Ne MGI and Ar MGI which are very different. For the Ar MGI case, the HXR signal from REs is observed from the beginning of CQ and it quickly increases within 1 ms (see figure 5(d)). For the Ne MGI case, the increase of the HXR signal is much more delayed, closer to the mid-CQ, and less steep (see figure 5(d)). This indicates that fewer seed REs enter into the CQ after Ne MGI and as a result they are accelerated to higher energy. This poorer seeding of REs is not understood yet, because Ne MGI causes faster TQ

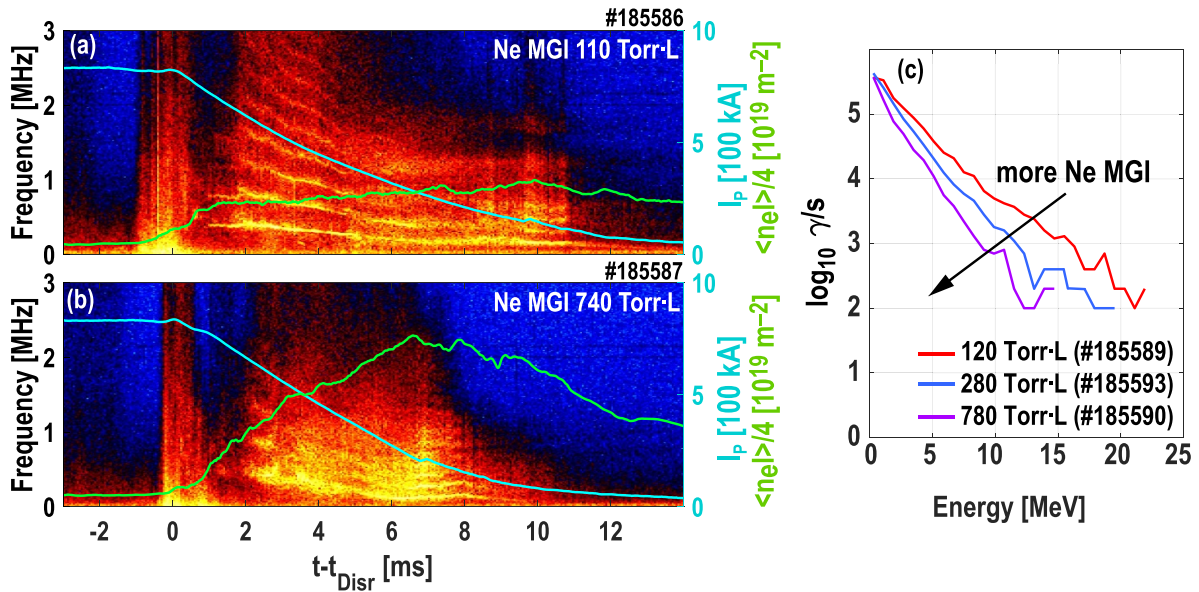


**Figure 4.** (a) and (b) spectrograms of toroidal magnetic field fluctuations after 110 Torr-L and 740 Torr-L of Ne MGI, respectively. Overplotted are plasma current  $I_p$  and line-integrated electron density  $\langle n_e l \rangle$ ; (c) dependence of the HXR bremsstrahlung spectra from REs obtained over the CQ (integration window is 10 ms after the disruptions) on the Ne MGI amount.

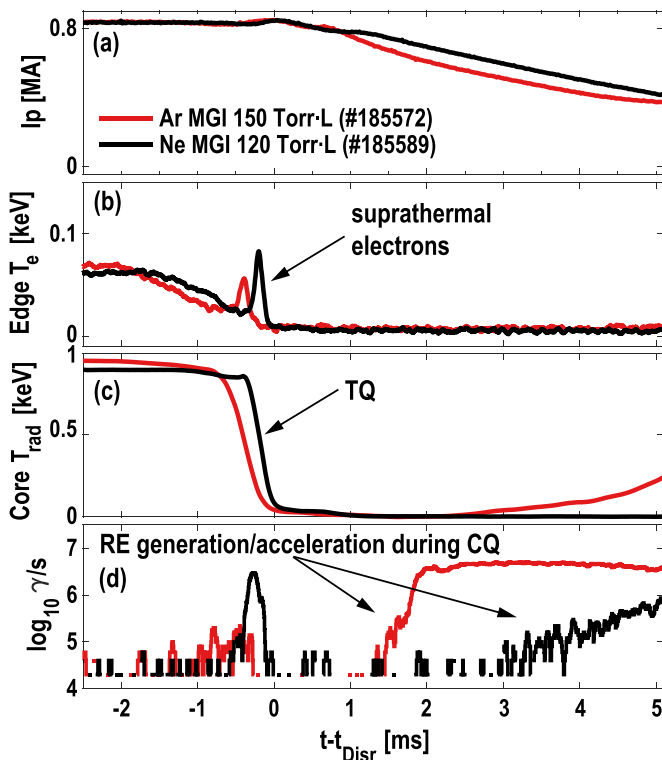


**Figure 5.** Comparison of plasma signals during disruptions after Ne MGI and Ar MGI. (a) Plasma current, (b) electron temperature by an edge ECE channel, (c) core plasma cooling by the 3rd harmonic broadband ECE, (d) HXR flux by the GRI.

than Ar MGI (0.3 ms vs 0.5 ms, as seen in figure 5(c)), which is expected to be favorable for the primary RE generation [34]. Besides possible poor initial seeding during the TQ, worse post-TQ survival of seed REs caused by MHD instabilities during the flattening of the current profile may be another

reason. This worse survival would explain no effect of shorter TQ as well as more peaked ECE and HXR signals at  $t = 0$  in figures 5(b) and (d), potentially associated with stronger RE seeding after Ne MGI. The seed REs are presently not well diagnosed at DIII-D due to the lack of measurements in the energy range from tens to hundreds keV, thus it is difficult to draw a conclusion whether Ne MGI indeed supplies fewer seed REs into the CQ.

In short, the role of Alfvénic instabilities is assumed to be less important than a small number of seed REs entering into the CQ after Ne MGI. But this reduced inventory of seed REs has no clear explanation yet.

**5.2.2. Disruptions caused by  $D_2$  MGI.**  $D_2$  MGI is another injection known to produce no sustained RE beams in DIII-D. Its study on the presence of Alfvénic instabilities is also important since a low-Z injection is considered to be the primary mean to suppress the RE generation in ITER. The experiment shows that the lack of the RE beam cannot be explained by instabilities increasing the RE loss during the CQ. As seen in figure 6(a), no instabilities and no RE loss are observed after  $D_2$  MGI. No signals from confined REs can be measured too. We explain this phenomenon by too slow plasma cooling during the TQ which causes slow increase in resistivity, small induced electric field and suppressed RE generation. Measurements of the plasma cooling after Ar MGI and  $D_2$  MGI shown in figure 6(b) support this hypothesis.  $D_2$  MGI causes a TQ by factor of 3 longer than Ar MGI (1.5 ms compared to 0.5 ms, respectively). An unusually wide  $I_p$  spike of about 2 ms can be also seen in figure 6(a). The duration of the CQ after  $D_2$  MGI is also longer than for other injections: about 8 ms compared to typical 5 ms. A survey of disruptions caused by  $D_2$  MGI shows that such an injection often does not ultimately disrupt the usual RE



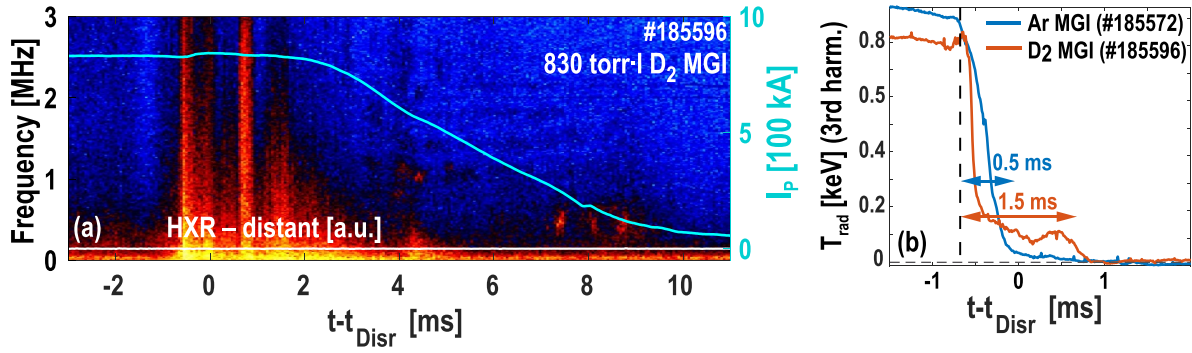


**Figure 6.** (a) Magnetic spectrogram during the CQ after D<sub>2</sub> MGI, (b) core plasma cooling by 3rd harmonic broadband ECE diagnostic.

target plasma in DIII-D: there are numerous observations of a staggered loss of the plasma thermal energy and very long CQ up to tens of ms with many small  $I_p$  spikes along the way.

## 6. Polarization and toroidal mode number of instabilities

### 6.1. Motivation

A recent upgrade of the RF diagnostic on DIII-D [16] provided previously missing measurements of the polarization and toroidal mode number of instabilities. The polarization data is useful to analyze whether the Alfvénic instabilities are of a shear (such as TAEs, global Alfvén eigenmodes (GAEs), etc) or compressional (such as CAEs) nature. The toroidal mode number is important to verify the validity of models such as the one developed in [13]. However, we should note that these are measurements at the edge, thus the information about the internal mode structure can be lacking.

### 6.2. Experiment

Plasma and injection parameters in this experiment are the same as in the  $B_T$  experiment presented in section 3.

The polarization of magnetic fluctuations is shown in figure 7(a). It is calculated as a dimensionless ratio of toroidal to poloidal fluctuations  $\delta B_T / \delta B_P$  using two orthogonal loops of the RF diagnostic. The corresponding magnetic spectrogram can be found in figure 1(b). It can be seen that the polarization is predominantly toroidal (compressional) over the area with instabilities. Insufficient resolution of separate modes can be likely explained by closely-spaced and relatively short modes. The mean polarization is presented in figure 7(b). It is obtained using a masking technique by separation of modes from the background in the magnetic spectrograms (by choosing regions with cross-power above 65% of the maximum cross-power) and calculating an average polarization over the same time–frequency region in polarization plots. The mean polarization linearly increases as  $B_T$  decreases, suggesting that the Alfvénic instabilities become more compressional.

The toroidally separated RF loops allow us to calculate the toroidal mode numbers of Alfvénic instabilities as shown in figure 7(c). Fast dynamics of the CQ and closely-spaced modes complicate this analysis too, though modes from  $n = -1$  to  $n = 1$  can be still seen. Analysis of available discharges shows that  $n = -1$  is often the lowest frequency mode,  $n = 0$  seems to be the most dominant mode (more on that in the discussion), and higher modes are often seen at higher frequencies (up to  $n = 2$  in one discharge with Ar MGI and two discharges with high amounts of Ne MGI).

### 6.3. Discussion and conclusions

The polarization measurements are consistent with previous estimates and modeling suggesting that the kinetic instabilities observed during the CQ are CAEs [10, 13]. However, we should note once again that these are measurements at the edge, thus they are not necessarily representative of the polarization deeper in the plasma, where the modes may be localized. Experimental and theoretical studies of CAEs and GAEs driven by fast ions show what both have large compressional component at the edge even though dominant polarizations in the core are very different ( $\delta B_T / \delta B_P \gg 1$  for CAEs and  $\delta B_T / \delta B_P \ll 1$  for GAEs) [49–52].

In the measured frequency range GAEs as the candidate instability can be excluded for modes observed above and near  $f_{ci}$ , since shear waves would be evanescent at such frequencies. However, both CAEs and GAEs can be driven at frequencies below  $f_{ci}$ .

Excitation of GAEs at low frequencies can actually explain a few exceptional cases where spectrograms do not exhibit modes tracking in the same direction. For example, figure 8(a) shows two lowest modes changing their frequency in the opposite directions during  $t \approx 5$ –7 ms. This behavior cannot be explained by evolving CAEs since the dispersion relation for CAEs states  $\omega(t) \approx kv_A(t)$  (where  $k$  is a wave number), i.e. all spectral lines must evolve parallel to one another, since the time dependence does not depend on the mode numbers. Conversely, shear modes such as GAEs are known to exhibit spectral lines evolving differently since their dispersion relation  $\omega(t) \approx k_{\parallel}(t)v_A(t)$  (where  $k_{\parallel}$  is a parallel wave number) can have different time evolution for different  $m$  numbers, since  $k_{\parallel}(t) = (n - m/q(t))/R$ , where  $n$ ,  $m$  are toroidal and poloidal

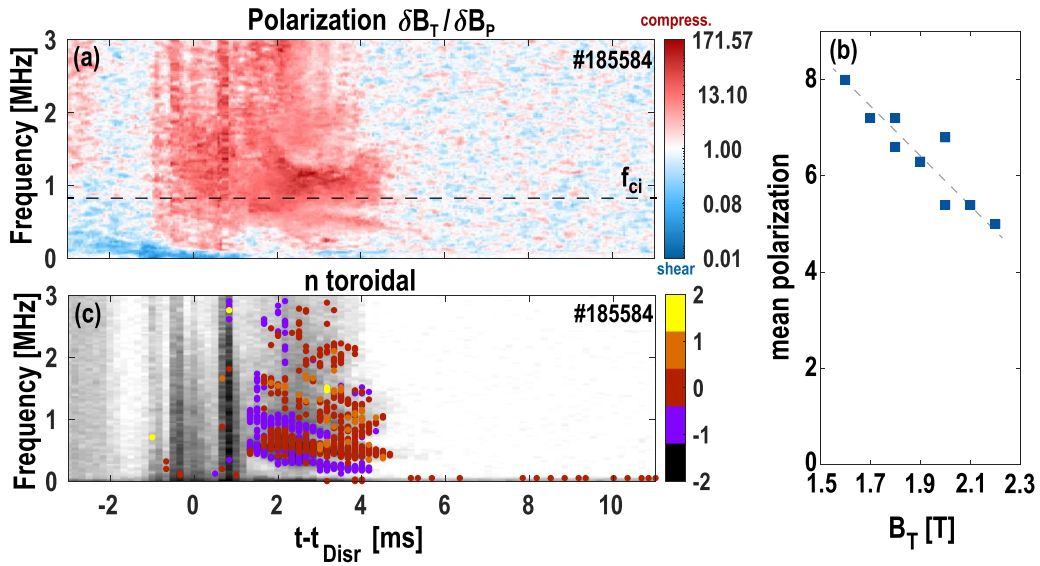


**Figure 7.** (a) Polarization of magnetic instabilities.  $f_{\text{ci}}$  is calculated assuming that  $\text{Ar}^+$  is the dominant species across the RE beam; (b) mean polarization calculated over the presence of modes (the dash line is to guide the eye only); (c) toroidal mode number of magnetic instabilities.

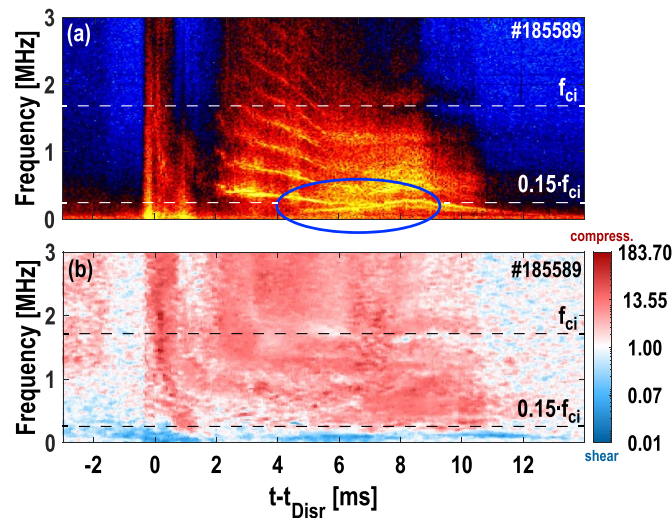


**Figure 8.** (a) Spectrogram of magnetic fluctuations showing an example of two lowest frequency modes evolving in different directions during  $t \approx 5\text{--}7$  ms, (b) polarization of magnetic fluctuations  $\delta B_T / \delta B_P$ .  $f_{\text{ci}}$  is calculated assuming that  $\text{Ne}^+$  is the dominant species over the RE beam.

mode numbers, respectively,  $q$  is a safety factor, and  $R$  is a major radius. Excitation of GAEs at lower frequencies would be also consistent with the transition from compressional to shear polarization seen at lower frequencies in figure 8(b).

Regarding the measurements of the toroidal mode number of kinetic instabilities, observation of  $n = 0$  mode seems to be doubtful. At first, excitation of this mode is not predicted by the existing model of CAEs driven by REs in DIII-D [13]. Secondly,  $n = 0$  mode prevents change in the toroidal angular momentum of runaways [53] which would suppress their radial transport. Since there are only three toroidal RF loops available for mode fitting, and the loops are closely spaced, it is possible that close modes are not robustly distinguished.

This is particularly true for modes quickly evolving during disruptions; also a small circular quenching plasma displaced to the centerpost provides relatively weak magnetic signals, which increases chances to pick up noise.

Additional analysis of lower frequency modes using an array of regular DIII-D magnetic probes (with the maximum cut-off at about 100–200 kHz), shows good fit for  $n = -1$  and  $n = 1$  modes, but much less plausible result for  $n = 0$ . A database study using the same probes finds that  $n = 0$  mode is often detected during the CQ, even in disruptions without any signs of kinetic instabilities or REs. This does not allow us to completely rule out the observation of instability  $n = 0$  mode, but indicates high probability that this signal can be seen by other

**Table 1.** List of all analyzed disruptions on presence of Alfvénic instabilities during the CQ on DIII-D. PI = ‘killer’ pellet injection, MGI = massive gas injection, SPI = shattered pellet injection.

Primary injection	RE beam	Instabilities	Comment
Ar PI	mostly ✓	mostly ×	Instabilities are rare, but no RE beam in such cases Favorable for RE beam: high $B_T$ ( $\geq 2.2$ T), low $I_P$ ( $< 1.2$ MA), high $T_e$ ( $\geq 8$ keV)
Ar MGI	✓/×	✓	Typically instabilities always present For RE beam: same as for Ar PI, qty $\geq 150$ Torr·L
Ne MGI	×	✓	No RE beam even for qty $> 1100$ Torr·L
Ne SPI	×	✓	Elongated IWL and Super-H targets surveyed
D <sub>2</sub> MGI	×	×	Plasma cooling is too slow to generate REs
D <sub>2</sub> SPI	×	✓	Instabilities only for Super H-mode target
Ne + D <sub>2</sub> SPI	×	✓	Instabilities only for Super H-mode target
C influx	×/✓	✓/×	No instabilities at high $T_e$ ( $\geq 8$ keV)
solid plastic pellet	×	✓	Only Super H- and Hybrid mode surveyed
C + W shell pellet	×	✓	Only Super H- and Hybrid mode surveyed
C + B shell pellet	×	✓	Only Super H- and Hybrid mode surveyed

reasons, for example, due to correlated noise (e.g. from choppers of poloidal field coils) or changing plasma equilibrium.

## 7. Summary and conclusions

In this work we documented the generation of sustained RE beams and parameters of RE-driven Alfvénic instabilities (presumably increasing RE loss from the plasma) during the CQ depending on the toroidal magnetic field, core plasma temperature, and species of material injection used to deliberately trigger the disruptions. It was observed that these instabilities almost always play a role in non-sustained RE beams, but this effect depends on parameters of the disruption.

It was found that lower magnetic field leads to increased RE energy, increased power and energy of Alfvénic instabilities and no sustained RE beam if the maximum RE energy is above 15 MeV (corresponds to  $B_T$  below 1.8 T). This is presumably caused by decreasing conversion of thermal to RE current as  $B_T$  decreases and acceleration of fewer REs to higher energy which is favorable for the excitation and greater energy of instabilities. As discussed in section 3, this decreased conversion can be explained by different reasons, including the presence of Alfvénic and high-frequency whistler instabilities, both favoring low  $B_T$ , or by on-axis current decreasing with  $B_T$ .

The increased core plasma temperature leads to an opposite and more pronounced effect: at  $T_e = 8$  keV the RE population is low energetic (max  $E_{RE} < 3$  MeV) and no instabilities can be observed, which can also be explained by increased current conversion.

Analysis of disruptions caused by Ne MGI and D<sub>2</sub> MGI, typically producing no sustained RE beams and abandoned in favor of the Ar injection in the RE experiments on DIII-D, shows that Ne MGI leads to highly energetic RE population ( $> 13$ – $23$  MeV) and the most clear and longest-duration (though moderately-energetic) instabilities of all cases studied. The increasing amount of Ne decreases the energy of REs, but they can still drive significant Alfvénic instabilities. However, poor RE seeding or poor survival of seed REs after Ne

MGI may also be responsible for non-sustained RE beams. The injection of D<sub>2</sub> MGI, also leading to no sustained RE beams, was not found to be related to Alfvénic instabilities: no signs of instabilities and no REs are measured during the CQ, which can be explained by too slow plasma cooling during the thermal quench.

The frequency dependence of instabilities on the toroidal magnetic field is as expected for Alfvénic instabilities. The dependence on the ion (electron) density is consistent with Alfvénic instabilities, but it is not possible to fully verify this due to diagnostic constraints. The measured edge polarization and toroidal mode numbers are compatible with the modeling predicting excitation of CAEs, but the measurements can not rule out shear GAEs in the range of  $f < f_{ci}$  either, since similar modeling and measurements of fast-ion-driven modes find compressional polarization at the edge for both CAEs and GAEs. Furthermore, examples of observed spectral lines evolving in different directions can not be straightforwardly explained if all modes were CAEs. Instead, this phenomenon could indicate that a low frequency subset of the Alfvénic activity is a shear wave, such as a GAE.

The survey of all disruptions studied on DIII-D, including the ones not discussed in this work, is given in table 1. It can be seen that there is always correlation between the presence of Alfvénic instabilities during the CQ and lack of sustained RE beam. The only outlier is D<sub>2</sub> MGI, though we expect that similar to D<sub>2</sub> SPI, it can still drive Alfvénic waves if a high-energy/high-current target plasma is used.

This survey also shows that reactor-relevant high plasma temperature and magnetic field are favorable for sustained RE beams. However, we consider that direct extrapolation of these results to ITER would be too straightforward. At first, reactor-relevant plasma current and low-Z impurity injection would be favorable for non-sustained RE beams, however, the magnitude of this counter-effect is unclear. And secondly, comprehensive modeling is necessary to weigh and better understand every dependence found and correctly extrapolate from DIII-D to ITER parameters. We should also point out that even if natural RE-driven CAEs and/or GAEs cannot prevent

RE generation, an external launch of similar waves using an antenna is still worth considering.

In future we plan to experimentally investigate RE generation after D<sub>2</sub> MGI/SPI in high-current/high-energy target plasma scenarios. A closer look at RE generation after Ne injections, including the RE seed formation, is also needed to better understand the physics of this process and derive more clear dependencies. Both experimental and simulation work is planned to study applicability of externally launched waves for RE dissipation.

To improve the existing model of RE-driven CAEs, and further understand the mode excitation mechanism and the dependence of mode growth on the plasma condition, we plan to use a kinetic-MHD code, like M3D-C1 [54] or MEGA [55], to do first-principle simulation to calculate the eigenmode structure, growth rates and frequencies to compare with experiments. The collisional damping of the mode will be included with the model described in [13]. We will also carry out a non-linear simulation to study the diffusion of REs due to perturbed magnetic fields, and test whether such modes can be driven in ITER scenarios.

### Acknowledgment

The authors are grateful to Max Austin and Deyong Liu for the diagnostic support, Ted Strait for the fruitful discussion on magnetic measurements, and Geri Papp for pointing out to the work on TAEs. This material is based upon work supported by the U.S. Department of Energy, Office of Science, Office of Fusion Energy Sciences, using the DIII-D National Fusion Facility, a DOE Office of Science user facility, under Awards DE-FC02-04ER54698, DE-FG02-07ER54917, DE-SC0021624, DE-SC0020337, DE-SC0018270, DE-AC02-09CH11466.

### Disclaimer

This report was prepared as an account of work sponsored by an agency of the United States Government. Neither the United States Government nor any agency thereof, nor any of their employees, makes any warranty, express or implied, or assumes any legal liability or responsibility for the accuracy, completeness, or usefulness of any information, apparatus, product, or process disclosed, or represents that its use would not infringe privately owned rights. Reference herein to any specific commercial product, process, or service by trade name, trademark, manufacturer, or otherwise, does not necessarily constitute or imply its endorsement, recommendation, or favoring by the United States Government or any agency thereof. The views and opinions of authors expressed herein do not necessarily state or reflect those of the United States Government or any agency thereof.

### Appendix. Additional plasma signals during the CQ

In this appendix we present plasma signals which may be useful to the interested reader for the initial modeling of RE

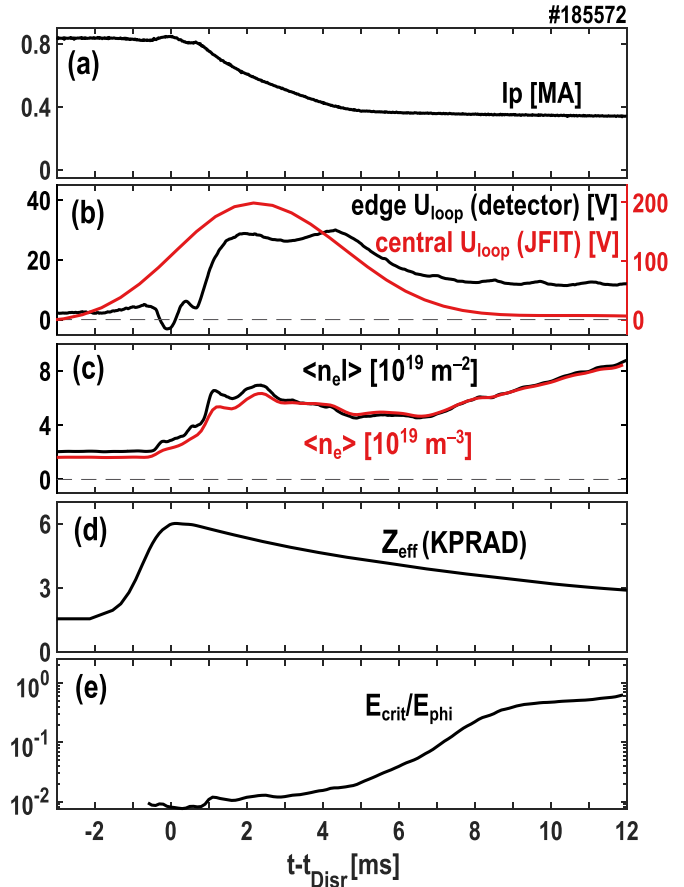


**Figure A1.** (a) Plasma current, (b) edge and central loop voltages, (c) line-integrated and line-averaged electron densities, (d) effective plasma charge, (e) the ratio of the Rosenbluth–Putvinski critical field to induced electric field.

generation and Alfvénic drive. We also encourage all interested parties to contact the authors to discuss any additional input needed.

Figure A1 shows the traces of the plasma current, loop voltage, line-integrated and line-averaged electron densities, effective plasma charge, and the ratio of the critical electric field to induced electric field in discharge #185572 (presented earlier in section 3). The plasma current ( $I_p$ ) is measured by magnetic probes inside the vessel which provides the best time resolution and also compensates the vessel currents. The edge loop voltage ( $U_{loop}$ ) is measured by a detector at the wall. Since the current profile changes during the disruption,  $U_{loop}$  is expected to be radius-dependent. The loop voltage in the central plasma region is estimated using the JFIT code, which calculates the current distribution by fitting distributed current elements [56]. For slow time scales (about 1 ms) it provides reasonable estimations of the central  $U_{loop}$  [57]. The line-integrated electron density ( $\langle n_e l \rangle$ ) is measured using the mid-plane radial chord of the CO<sub>2</sub>-interferometer. The line-averaged electron density ( $\langle n_e \rangle$ ) is calculated from ( $\langle n_e l \rangle$ ) using EFIT reconstructions of the plasma geometry. The effective plasma charge ( $Z_{eff}$ ) cannot be routinely measured during impurity-induced disruptions due to high radiation level compromising visible bremsstrahlung and charge

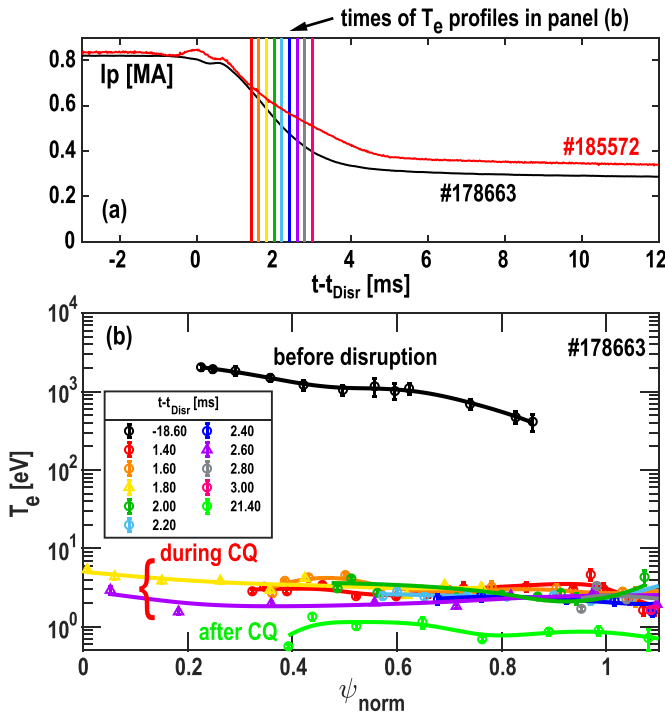


**Figure A2.** (a) Plasma current and times of the temperature profiles, (b) temperature profiles by the Thomson scattering during the CQ mapped to the normalized poloidal magnetic flux.

exchange recombination signals used for  $Z_{\text{eff}}$  calculations. Instead,  $Z_{\text{eff}}$  is estimated using the 0D code KPRAD, which models impurity deposition and radiation [58–60]. Notably, the RE generation was not modeled by KPRAD, it assumes a complete CQ without formation of the RE plateau. The ratio of the critical electric field to induced electric field ( $E_{\text{crit}}/E_{\text{phi}}$ ) is calculated using the Rosenbluth–Putvinski critical field [61] estimated from  $\langle n_e \rangle$  and  $Z_{\text{eff}}$  and the induced electric field estimated from the central  $U_{\text{loop}}$ . The Connor–Hastie critical field [62] is not shown as it does not take into account bound electrons which are important for the argon massive injection.

Figure A2 presents the electron temperature profiles during the CQ for a similar RE discharge (#178663). These profiles are measured by the Thomson scattering diagnostic, and they only occasionally become available during the CQ when the lasers' pulses overlaps with the CQ. Since #178663 was a discharge disrupted by an Ar killer pellet, we do not provide the electron density profiles to avoid confusing the reader (the discharge #185572 employed Ar MGI in the amount of  $10\times$  greater). However, we assume the temperature dynamics to be similar during the CQ in these two discharges since the same picture is observed during typical CQs in DIII-D: the temperature profile is flat and decreases from tens of eV at the very beginning of the CQ to a few eV at the end

## ORCID iDs

A. Lvovskiy <https://orcid.org/0000-0002-3649-1169>  
 C. Paz-Soldan <https://orcid.org/0000-0001-5069-4934>  
 N.W. Eidietis <https://orcid.org/0000-0003-0167-5053>

A. Dal Molin <https://orcid.org/0000-0003-0471-1718>  
 G.H. DeGrandchamp <https://orcid.org/0000-0002-1363-9570>  
 E.M. Hollmann <https://orcid.org/0000-0002-6267-6589>  
 J.B. Lestz <https://orcid.org/0000-0002-6975-1537>  
 C. Liu <https://orcid.org/0000-0002-6747-955X>  
 M. Nocente <https://orcid.org/0000-0003-0170-5275>  
 X.D. Du <https://orcid.org/0000-0001-6127-2825>

## References

- [1] Loarte A. 2020 Required R and D in existing fusion facilities to support the ITER research plan *ITER Technical Report ITR-20-008*
- [2] Breizman B.N., Aleynikov P., Hollmann E.M. and Lehnen M. 2019 *Nucl. Fusion* **59** 083001
- [3] Lehnen M., Campbell D.J., Hu D., Kruezi U. and Luce T.C. 2018 R&D for reliable disruption mitigation in ITER *IAEA Fusion Energy Conf. (Ahmedabad, India, 22–27 October 2018)* (International Atomic Energy Agency, Division of Physical and Chemical Sciences, Physics Section, Vienna, Austria) EX/P7-12 (available at: <https://nucleus.iaea.org/sites/fusionportal/Shared%20Documents/FEC%202018/fec2018-preprints/preprint0318.pdf>)
- [4] Paz-Soldan C., Eidietis N.W., Liu Y.Q.Q., Shiraki D., Boozer A.H., Hollmann E.M., Kim C.C. and Lvovskiy A. 2019 *Plasma Phys. Control. Fusion* **61** 054001
- [5] Reux C. et al 2021 *Phys. Rev. Lett.* **126** 175001
- [6] Paz-Soldan C. et al 2021 *Nucl. Fusion* **61** 116058
- [7] Weisberg D.B., Paz-Soldan C., Liu Y.Q., Welander A. and Dunn C. 2021 *Nucl. Fusion* **61** 106033
- [8] Tinguely R.A. et al 2021 *Nucl. Fusion* **61** 124003
- [9] Choudhury H., Battey A., Paz-Soldan C., Lvovskiy A. and Akiyama T. 2022 Antenna-driven compressional Alfvén eigenmodes in relativistic electron beam plasmas [BP11.00059] *Bulletin of the American Physical Society* (Spokane, WA: American Physical Society)
- [10] Lvovskiy A. et al 2018 *Plasma Phys. Control. Fusion* **60** 124003
- [11] Heinrich P. 2021 Investigations of Alfvénic activity during the current quench in ASDEX upgrade *PhD Thesis Technische Universität München*
- [12] Lier A., Papp G., Lauber P.W., Embreus O., Wilkie G.J. and Braun S. 2021 *Nucl. Fusion* **61** 086003
- [13] Liu C., Brennan D.P., Lvovskiy A., Paz-Soldan C., Fredrickson E.D. and Bhattacharjee A. 2021 *Nucl. Fusion* **61** 036011
- [14] Liu C., Bhattacharjee A. and Jardin S.C. 2022 Kinetic-MHD simulation of compressional Alfvén eigenmodes excited by runaway electrons in current quench *IAEA 2nd Technical Meeting on Plasma Disruptions and Their Mitigation (Saint-Paul-lez-Durance, France, 19–22 July 2022)*
- [15] Luxon J. 2002 *Nucl. Fusion* **42** 313
- [16] Degrandchamp G.H., Thome K.E., Heidbrink W.W., Holmes I. and Pinsker R.I. 2021 *Rev. Sci. Instrum.* **92** 033543
- [17] Cooper C.M., Pace D.C., Commaux N., Eidietis N.W., Hollmann E.M. and Shiraki D. 2016 *Rev. Sci. Instrum.* **87** 11E602
- [18] Pace D.C., Cooper C.M., Taussig D., Eidietis N.W., Hollmann E.M., Riso V., Van Zeeland M.A. and Watkins M. 2016 *Rev. Sci. Instrum.* **87** 043507
- [19] Paz-Soldan C. et al 2017 *Phys. Rev. Lett.* **118** 255002
- [20] Paz-Soldan C. et al 2018 *Phys. Plasmas* **25** 056105
- [21] Lvovskiy A. et al 2020 *Nucl. Fusion* **60** 056008
- [22] Lvovskiy A., Paz-Soldan C., Eidietis N., Dal Molin A., Nocente M., Cooper C., Rigamonti D., Tardocchi M. and Taussig D. 2022 *Rev. Sci. Instrum.* **93** 113524

- [23] Dal Molin A. et al 2018 *Rev. Sci. Instrum.* **89** 101134
- [24] Heidbrink W.W. 1986 *Rev. Sci. Instrum.* **57** 1769–70
- [25] Austin M.E. and Lohr J. 2003 *Rev. Sci. Instrum.* **74** 1457–9
- [26] Garstka G., Ellis R. and Austin M. 2001 *Fusion Eng. Des.* **53** 97–103
- [27] Carlstrom T.N., Ahlgren D.R. and Crosbie J. 1988 *Rev. Sci. Instrum.* **59** 1063
- [28] Hender T.C. et al 2007 *Nucl. Fusion* **47** S128–202
- [29] Chen Z.Y. et al 2013 *Plasma Phys. Control. Fusion* **55** 035007
- [30] Zeng L., Chen Z., Dong Y., Koslowski H., Liang Y., Zhang Y., Zhuang H., Huang D. and Gao X. 2017 *Nucl. Fusion* **57** 046001
- [31] Zeng L. et al 2013 *Phys. Rev. Lett.* **110** 235003
- [32] Svensson P., Embreus O., Newton S.L., Särkimäki K., Vallhagen O. and Fülöp T. 2021 *J. Plasma Phys.* **87** 905870207
- [33] Papp G., Lauber P.W., Schneller M., Braun S., Koslowski H.R. and Team T. 2014 *41st EPS Conf. on Plasma Physics (Berlin, Germany, 23–27 June 2014)*
- [34] Paz-Soldan C., Aleynikov P., Hollmann E., Lvovskiy A., Bykov I., Du X., Eidietis N. and Shiraki D. 2020 *Nucl. Fusion* **60** 056020
- [35] Hollmann E.M. et al 2013 *Nucl. Fusion* **53** 083004
- [36] Hollmann E.M. et al 2020 *Phys. Plasmas* **27** 042515
- [37] Reux C. et al 2015 *Nucl. Fusion* **55** 093013
- [38] Fülöp T., Pokol G., Helander P. and Lisak M. 2006 *Phys. Plasmas* **13** 062506
- [39] Pokol G., Fülöp T. and Lisak M. 2008 *Plasma Phys. Control. Fusion* **50** 045003
- [40] Fülöp T., Smith H.M. and Pokol G. 2009 *Phys. Plasmas* **16** 022502
- [41] Aleynikov P. and Breizman B. 2015 *Nucl. Fusion* **55** 043014
- [42] Liu C., Hirvijoki E., Fu G.Y., Brennan D.P., Bhattacharjee A. and Paz-Soldan C. 2018 *Phys. Rev. Lett.* **120** 265001
- [43] Ghai Y., Spong D.A., Beidler M.T. and del-Castillo-Negrete D. 2022 Modelling interaction of runaway electrons with whistler waves using KORC-AORSA model [PO05.00007] *Bulletin of the American Physical Society* (Spokane WA: American Physical Society)
- [44] Spong D.A. et al 2018 *Phys. Rev. Lett.* **120** 155002
- [45] Heidbrink W.W., Paz-Soldan C., Spong D.A., Du X.D., Thome K.E., Austin M.E., Lvovskiy A., Moyer R.A., Pinsker R.I. and Zeeland M.A.V. 2019 *Plasma Phys. Control. Fusion* **61** 014007
- [46] Smith H., Helander P., Eriksson L.G. and Fülöp T. 2005 *Phys. Plasmas* **12** 122505
- [47] Smith H.M. and Verwichte E. 2008 *Phys. Plasmas* **15** 072502
- [48] Aleynikov P. and Breizman B.N. 2017 *Nucl. Fusion* **57** 046009
- [49] Fredrickson E.D. et al 2006 *Phys. Plasmas* **13** 056109
- [50] Belova E.V., Gorelenkov N.N., Crocker N.A., Lestz J.B., Fredrickson E.D., Tang S. and Tritz K. 2017 *Phys. Plasmas* **24** 042505
- [51] Belova E.V., Fredrickson E.D., Lestz J.B. and Crocker N.A. 2019 *Phys. Plasmas* **26** 092507
- [52] Lestz J.B., Belova E.V. and Gorelenkov N.N. 2021 *Nucl. Fusion* **61** 086016
- [53] Heidbrink W.W. 2008 *Phys. Plasmas* **15** 055501
- [54] Liu C., Jardin S.C., Qin H., Xiao J., Ferraro N.M. and Breslau J. 2022 *Comput. Phys. Commun.* **275** 108313
- [55] Wang J., Todo Y., Wang H. and Wang Z.X. 2020 *Nucl. Fusion* **60** 112012
- [56] Humphreys D.A. and Kellman A.G. 1999 *Phys. Plasmas* **6** 2742
- [57] Hollmann E.M., Commaux N., Eidietis N.W., Lasnier C.J., Rudakov D.L., Shiraki D., Cooper C., Martin-Solis J.R., Parks P.B. and Paz-Soldan C. 2017 *Phys. Plasmas* **24** 062505
- [58] Whyte D.G. et al 1997 Energy balance, radiation and stability during rapid plasma termination via impurity pellet injections on DIII-D *24th European Conference on Controlled Fusion and Plasma Physics (9–13 June 1997)* vol 21A (Berchtesgaden, Germany: European Physical Society) p 1137
- [59] Whyte D.G. et al 2003 *J. Nucl. Mater.* **313–316** 1239–46
- [60] Hollmann E.M., Parks P.B. and Scott H.A. 2008 *Contrib. Plasma Phys.* **48** 260–4
- [61] Rosenbluth M.N. and Putvinski S.V. 1997 *Nucl. Fusion* **37** 1355–62
- [62] Connor J.W. and Hastie R.J. 1975 *Nucl. Fusion* **15** 415–24